Investigating Variability of Antarctic Sea Ice on Subseasonal-to-Seasonal Time Scales

MIDN 1/C Aspen S. Bess[1], Prof. Bradford S. Barrett[1], and Prof. Gina Henderson[1]
[1]Oceanography Dept., U.S. Naval Academy, Annapolis MD 21402

Introduction

Intraseasonal tropical climate variability has important implications on mid- and high- latitude climate. Recent studies have found modulation of a number of weather processes in the Northern Hemisphere, such as snow depth (Guan et al. 2012; Barrett et al. 2015; Li et al. 2016), sea ice concentration (Henderson et al. 2014), precipitation (Donald et al. 2006), atmospheric rivers (Higgins et al. 2000), and air temperature (Vecchi and Bond 2004; Seo et al. 2016; Zhou et al. 2016). In such studies, the leading mode of tropical intraseasonal variability, the Madden-Julian Oscillation (MJO), has tended to lag tropical convection by approximately 7 days. However, such consensus is still absent when considering the relationship and lag between the MJO and the Antarctic atmosphere. Flatau and Kim (2013) suggested a lag of 7-10 days between the Antarctic Oscillation (AAO) and the MJO, while Fauchereau et al. (2016) and Henderson et al. (2018) suggested important lags between MJO convection and extratropical circulation out to 20 days.

This study builds on previous work by **further examining the time-lagged response of Southern Hemisphere tropospheric circulation to tropical MJO forcing**, with specific focus on the latitude belt associated with the AAO, during the months of June (Austral winter) and December (Austral summer).

Tropical-Antarctic teleconnections

What is the MJO?

- A large-scale mode of atmospheric tropical variability
- Moves generally eastward around the equator on a time scale of 30-60 days.
- Most active in the eastern hemisphere (Indian Ocean to Western Pacific Ocean).

How is the MJO connected to Antarctica?

- Large-scale latent heat release of the MJO convection excites poleward-moving Rossby Waves
- Those Rossby waves modulate surface pressure and circulation, which then modulate ice (Fig. 1)

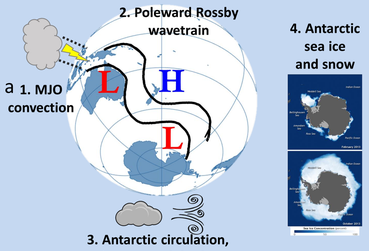

***Figure 1**: Schematic the MJO's influence from the tropics to the extratropics*

Data & Methods

- This study utilized the National Snow and Ice Data Center (NSIDC) daily climate record of Passive Microwave Sea Ice Concentration, version 3
  - Daily observations of sea ice concentration from 1989 to 2018 were considered.
  - Sea ice area was calculated from concentration by multiplying the concentration for all grid boxes with concentration > 0.00001 by the area the box (25 km x 25 km).
  - Sea ice extent by sector was determined from concentration if the concentration > 0.15 for a grid box in a specific sector.
  - Daily change in sea ice concentration (ΔSIC) was determined by subtracting the given day from the previous day to calculate the change in ice concentration.
  - Positive or negative ΔSIC represents a net gain or loss of sea ice concentration respectively.

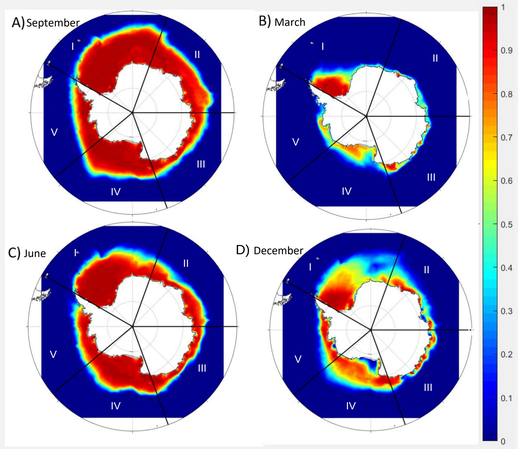

***Figure 2:** Southern Hemisphere 30-year average ice concentration for a) September, the month of maximum sea ice extent, b) March, the month of minimum sea ice extent, and for the transitional months of June c) and December d). Sectors I-V refer to; I- Weddell Sea Sector, II- Indian Ocean Sector, III- Western Pacific Ocean Sector, IV- Ross Sea Sector and V- Bellingshausen & Amundsen Seas.*

- September displays maximum sea ice concentration with largest magnitudes located in the Weddell Sea Sector (Fig. 2a, sector I) .
- March displays minimum sea ice concentration with smallest values in the Indian Ocean Sector (Fig. 2b, sector II).
- June is a transitional month of sea ice concentration with highest values in the Weddell Sea Sector (Fig. 2c, sector I).
- December is also a transitional month with the lowest values in the Indian Ocean Sector (Fig. 2d, sector II).

Maximum & Minimum Sea Ice Extent Standard Anomalies: September and March

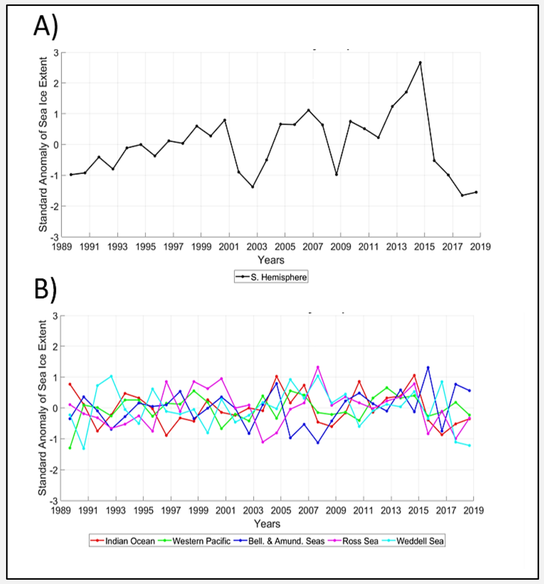

***Figure 3:** Standard anomalies for September from 1989-2018 for (a) Southern Hemisphere and (b) the five sectors; Indian Ocean, Western Pacific, Bellingshausen & Amundsen Seas, Ross Sea and Weddell Sea.*

- In September, the month of maximum sea ice concentration, the Southern Hemisphere is characterized by largely neutral sea ice concentration anomalies for the first 25 years of the period of record (Fig. 3a).
- The last five years however, show negative anomalies after a peak in 2014.
- When considering regional ice variability, the five sectors within Southern Hemisphere display variable anomalies among the first 25 years, with the last 5 years characterized by negative anomalies in most sectors.
- The Bellingshausen and Amundsen Seas sector (sector V) shows positive anomalies in most recent years (Fig. 3b, blue line).

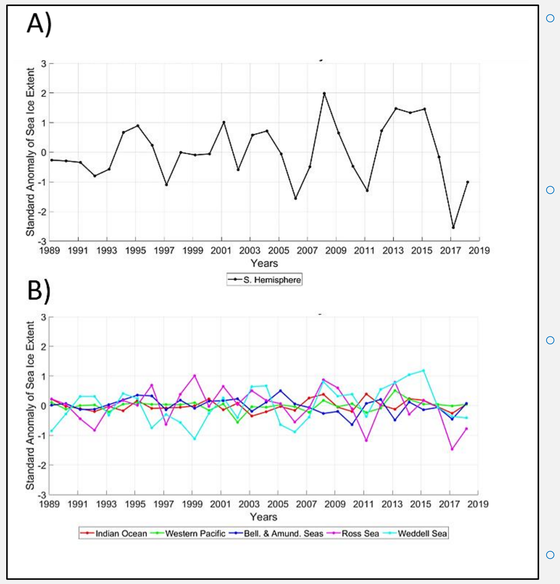

***Figure 4:** As in Fig. 3 for March.*

- In March, the month of minimum sea ice concentration, the Southern Hemisphere is characterized by largely neutral anomalies for the first 25 years of the period record (Fig. 4a).
- Sea ice concentration anomalies from 2008-2011 and 2015-2017 displayed negative anomalies after both having a maximum peak.
- When considering regional ice variability, the five sectors within Southern Hemisphere display variable anomalies among the first 27 years, with the following 2 years characterized by negative anomalies in most sectors.
- Every sector, besides Weddell Sea (sector I), demonstrated positive anomalies in 2018.

Sea Ice Concentration Change by Phase of MJO: June (left) and December (right)

- The month of June experiences the most positive ΔSIC over the 30-year period.
- When considering regional daily ice variability, every sector shows positive sea ice change within every phase. However, each sector and phase varies in magnitude of ΔSIC.
- The Weddell Sea sector (cyan) shows the most positive ΔSIC throughout, however, there is also as negative ΔSIC present throughout this sector in phases 3-7.
- The Western Pacific sector (green) shows the least positive daily ΔSIC, with phase 8 being the least overall.
- The Indian Ocean sector (red) shows the most positive ΔSIC in phase 6.
- Phase 1 and phase 8 show the smallest positive ΔSIC compared to the other phases.
- Phase 5 and phase 6 show the most positive ΔSIC in all sectors compared to other phases, while phase 3 in the Ross Sea (magenta) shows both positive and negative ΔSIC.

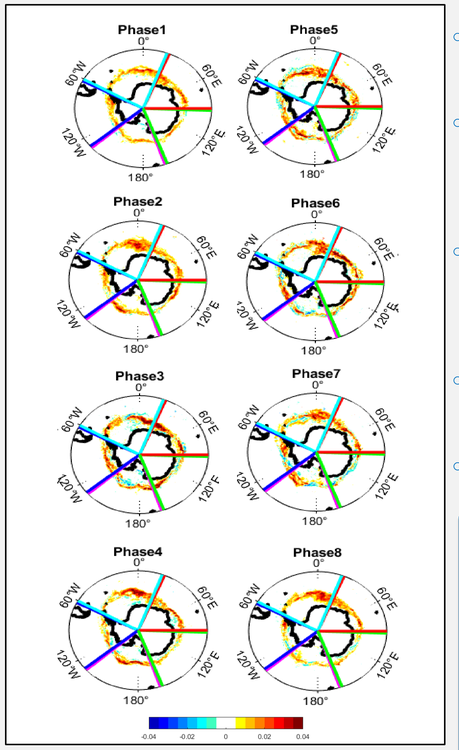

***Figure 5:** Daily change in sea ice concentration for June from 1989-2018 for the Southern Hemisphere and the five sectors; Indian Ocean (red), Western Pacific (green), Bellingshausen & Amundsen Seas (blue), Ross Sea (magenta) and Weddell Sea (cyan).*

- The month of December experiences predominantly negative ΔSIC over the 30-year period.
- When considering regional daily ice variability, every sector shows negative sea ice change within every phase. However, each sector and phase varies in magnitude of ΔSIC.
- The Weddell Sea sector (cyan) displays the most negative daily ΔSIC throughout, however, there is also a small area of positive ΔSIC in this sector in phases 1 and 8.
- The Western Pacific sector (green) shows the least positive daily ΔSIC with phase 8 being the least overall.
- Phase 3 and phase 4 show the most positive ΔSIC in the Weddell Sea (cyan).

Future work:

The next steps in this work include:

- Separating and normalizing positive and negative anomalies
- Analyzing MJO in all 12 months
- Exploring magnitudes of anomalies per sector
- Discovering time lags between MJO phase and ΔSIC

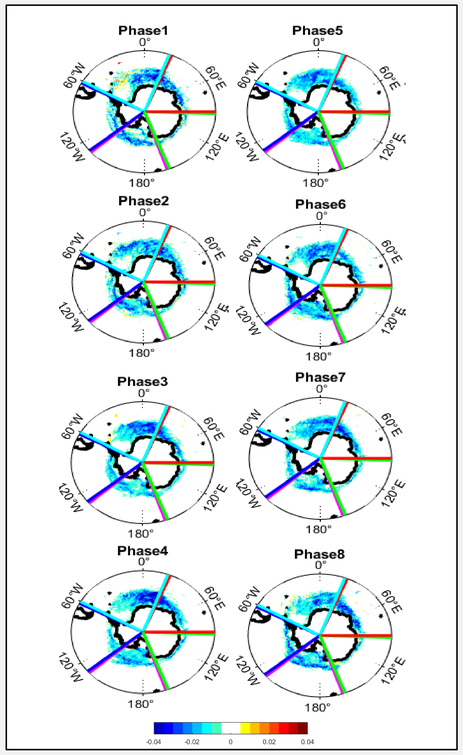

***Figure 6:** As in Fig. 5, but for for December*

Acknowledgements

The authors gratefully acknowledge support of this research from the NSF Office of Polar Programs (OPP), award no. 1821915.

References

Barrett, B. S., G. R. Henderson, and J. S. Werling, 2015: The influence of MJO on the intraseasonal variability of Northern Hemisphere spring snow depth. *J. Climate*, **28**, 7250-7262.

Donald, A., H. Meinke, B. Power, A. H. N. de Maia, M. C. Wheeler, N. White, R. C. Stone, and J. Ribbe (2006), Near-global impact of the Madden-Julian oscillation on rainfall. *Geophys. Res. Lett.*, **33**, L09704, doi:10.1029/2005GL025155.

Fauchereau, N. N., B.B. Pohl, and A.A. Lorrey, 2016: Extratropical impacts of the Madden–Julian Oscillation over New Zealand from a weather regime perspective. *J. Climate*, **29**, 2161–2175, doi: 10.1175/JCLI-D-15-0152.1.

Flatau M. and Y. J. Kim, 2013: Interaction between the MJO and polar circulations. J. Clim. 26: 3562–3574.

Guan, B., D. E. Waliser, N. P. Molotch, E. J. Fetzer, and P. J. Neiman, 2012: Does the Madden–Julian Oscillation influence wintertime atmospheric rivers and snowpack in the Sierra Nevada?. *Mon. Wea. Rev.*, **140**, 325–342, doi: 10.1175/MWR-D-11-00087.1.

Henderson, G. R., B. S. Barrett, and D. M. LaFleur, 2014: Arctic sea ice and the Madden-Julian Oscillation (MJO). *Climate Dyn.*, **43**, 2185-2196. doi:10.1007/s00382-013-2043-y.

Higgins, R. W., J.-K. E. Schemm, W. Shi, and A. Leetmaa (2000), Extreme precipitation events in the Western United States related to tropical forcing, *J. Climate*, **13**, 793–820.

Li, W., W. Guo, P. Hsu, and Y. Xue, 2016: Influence of the Madden–Julian oscillation on Tibetan Plateau snow cover at the intraseasonal time-scale. *Scientific Reports*, 6, 30456. http://doi.org/10.1038/srep30456.

Seo, K.-H., H. Lee, and D.W. Frierson, 2016: Unraveling the teleconnection mechanisms that induce wintertime temperature anomalies over the Northern Hemisphere continents in response to the MJO. *J. Atmos. Sci.*, **73**, 3557–3571, doi: 10.1175/JAS-D-16-0036.1.

Vecchi, G. A., and N. A. Bond (2004), The Madden-Julian Oscillation (MJO) and northern high latitude wintertime surface air temperatures. *Geophys. Res. Lett.*, **31**, L04104, doi:10.1029/2003GL018645.

Zhou, Y., Y. Lu, B. Yang, J. Jiang, A. Huang, Y. Zhao, M. La, and Q. Yang, 2016: On the relationship between the Madden-Julian Oscillation and 2 m air temperature over central Asia in boreal winter. *J.Geophys. Res. Atmos.*, **121**, 13,250-13,272.